Automatized Kinetic and Strain Field Based Calibration for a Thermoplastic Material Model using High-Speed Tensile Tests

Stefan Schilling, Philipp Suppinger, Dr. Peter Blome

Autoliv B.V. & Co. KG

1 Introduction

Current and future automotive development cycles are driven by the needs for lightweight designs, cost reductions, comfort- and safety improvements and the reduction of time-to-market. One way to cope with the listed challenges is the usage of thermoplastic materials for integrative designs of components. Among the challenges for passive safety supplier Autoliv to design thermoplastic components, which are placed in the load path of seatbelt components, is the strong dependency on loading velocity of the components. As crash situations are the most dominant load cases for design and functionality, a strong demand for predictive strain rate dependent material models is given. Strain rate effects are next to temperature- and humidity effects the major challenge concerning thermoplastics.
As an industrial demand for a comprehensive material database, it needs to be fast, efficient, economical and accurate. Also, the need for a fully automatized material model calibration process is expressed. To fulfill these demands a two-stage reverse engineering process fits test results to analytical approaches for a quasi-static and a strain rate dependent stress-strain response along with an analytic approach for modelling of visco-elasticity and strain rate dependent damage. The needed test results, to which the analytical parameters are fitted, consist of force-displacement as well as strainfield characteristics and were measured using a newly developed high-speed tensile testing device. This device is designed to get close to constant loading velocity of specimen resulting in strain rates up to $\dot{\varepsilon} = 320\ s^{-1}$. The accuracy of the test results is ensured by a wedge-to-wedge, self-locking coupling mechanism, a start-up length for acceleration travel of the tensile testing machine as well as a local force gauge. Especially by the local force gauge, consisting of strain gauges arranged as *Wheatstone* bridge, it is realized that oscillations in force signals of dynamic testing are minimized.
The automatized material model calibration routine fed with accurate test results from the high-speed tensile testing device shows promising results to further enhance simulation quality and predictability for the design of thermoplastic components in crash load cases.

2 Methodology of material model calibration using a reverse engineering process

Implementation of test results in material models is not always possible by analytical means, especially for plastic materials, where large deformations occur. As strain rate dependencies come in to play additionally, a reverse engineering process is needed to calibrate the material model such that the in-the-loop validation succeeds in comparing simulation to test results. A reverse engineering process developed in previous works [2], [3] is used and enhanced, along with recent version of ***MAT_SAMP-1** provided with LS-Dyna R10 [1].
The reverse engineering process bases on test results for three different loading velocities, where the first is to be considered as quasi-static and the two following need to be at higher strain rates. The respective test setups will be discussed later in Chapter 3.2.
The material ***MAT_SAMP-1** is expecting data points consisting of true stress and true plastic strain. As those data points are given in table-format, a strain rate dependency can be provided for the material model. Hence, an analytical description of the material stress behavior in dependency on plastic strain and strain rate needs to be found. As the material model is expecting true plastic strain as abscissa values, a strain rate dependent *Young*'s modulus can be provided to describe a visco-elastic behavior. Thus, an analytical function of *Young*'s modulus in dependency on strain rate $\dot{\varepsilon}$ needs to be found. And finally, two damage parameters of ***MAT_SAMP-1** are to be determined, one is rate dependent failure strain, the other is the increment of plastic strain between failure and rupture point. In other words, the first parameter is the beginning of material instability, the other parameter describes the material softening until element deletion is applied.

Concluding, the material model calibration process requires to solve the following relationships to describe the material behavior, given in Eq. 1 toEq. 3, where σ is the equivalent stress state, ε_{pl} the corresponding equivalent plastic strain and $\dot{\varepsilon}_{pl}$ the nominal plastic strain rate. Along with $\dot{E}$ as rate dependent *Young*'s modulus and E_0 as quasi-static *Young*'s modulus, as well as ε_{fail} as plastic failure strain and ε_{soft} as increment of plastic strain between failure and rupture strain.

$$\sigma = f\left(\varepsilon_{pl}, \dot{\varepsilon}_{pl}\right) \quad \text{Eq. 1}$$

$$\dot{E} = f(E_0, \dot{\varepsilon}) \quad \text{Eq. 2}$$

$$\varepsilon_{fail}, \varepsilon_{soft} = f(\dot{\varepsilon}) \quad \text{Eq. 3}$$

To cope with Eq. 1 toEq. 3, the following analytical functions are applied, where Eq. 5 bases on Eq. 4. Here, σ_0 is the quasi-static equivalent stress state with its coefficients φ_i with $i = 0 \ldots 4$ as well as the rate dependent equivalent stress state $\dot{\sigma}$ with its coefficients ξ_i with $i = 0 \ldots 4$ and $\dot{\varepsilon}_0$ the strain rate at quasi-static test velocity.

$$\sigma_0(\varepsilon_{pl}) = \left[\varphi_0 + \varphi_1 \cdot {\varepsilon_{pl}}^{\varphi_2}\right] \cdot \ln(\varphi_3 + \varepsilon_{pl}^{\varphi_4}) \quad \text{Eq. 4}$$

$$\dot{\sigma}(\dot{\varepsilon}_{pl}) = \sigma_0 \cdot \left[1 + \xi_0 \cdot \ln\left(\xi_1 + \frac{\dot{\varepsilon}_{pl}^{\xi_4}}{\dot{\varepsilon}_0}\right) \cdot e^{-\left[\frac{\xi_2 \cdot \varepsilon_{pl}}{\xi_3 + \ln\left(\xi_1 + \frac{\dot{\varepsilon}_{pl}^{\xi_4}}{\dot{\varepsilon}_0}\right)}\right]}\right] \quad \text{Eq. 5}$$

For Eq. 2, the following analytical approach (Eq. 6) is used to determine the rate dependent *Young*'s modulus $\dot{E}$ in dependency on quasi-static *Young*'s modulus E_0 and its coefficients ψ_i with $i = 0{,}1$

$$\dot{E}(\dot{\varepsilon}) = E_0 \cdot e^{\psi_0 \cdot \dot{\varepsilon}^{\psi_1}} \quad \text{Eq. 6}$$

Eq. 3 is solved without an analytical description, determining plastic failure strain ε_{fail} and increment of plastic strain ε_{soft} between failure and rupture strain individually for the two higher strain rates, later specified as medium- and high-speed strain rate.

The full set of 15 unknown parameters needs to be determined to describe the material behavior. The reverse engineering process uses force-displacement as well as strain-displacement characteristics from test results (Chapter 3) and optimizes the 15 unknown parameter such that the area between test- and simulation curve characteristics is minimized. This two-stage routine is fully automatized using python-scripts for data handling and LS-OPT as optimizer. The first stage determines the coefficients φ_i with $i = 0 \ldots 4$ for the quasi-static equivalent stress state σ_0 and passes information on to the second stage. Here, the rate dependent equivalent stress state $\dot{\sigma}$ with its coefficients ξ_i with $i = 0 \ldots 4$ as well as rate dependent *Young*'s modulus $\dot{E}$ with its coefficients ψ_i with $i = 0{,}1$, plastic failure strain ε_{fail} and increment of plastic strain ε_{soft} between failure and rupture strain are being solved. The second stage solves the before mentioned parameter as multi-objective optimization problem for the medium- and high-speed load cases. This two-stage iterative reverse engineering routine is illustrated in Fig. 1:

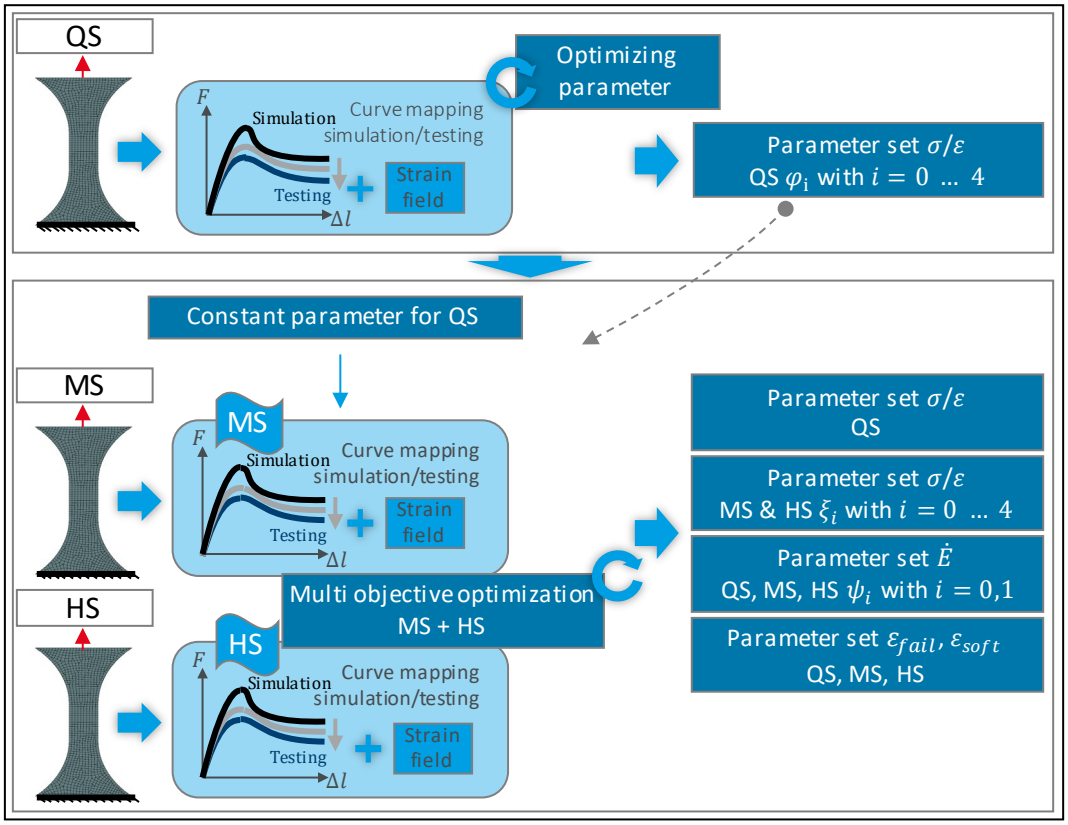

Fig. 1: Two-stage reverse engineering process to determine at first the quasi-static stress-strain relationship of material and at second as multi objective optimization the parameter of medium- and high-speed test velocities for the stress-strain, rate dependent Young's modulus and failure/softening relationships.

3 Experimental results using high-speed tensile testing device

A test device is developed which is specialized on high-speed tensile testing procedures. Its development is motivated from high-speed tensile test results, where oscillations in force-time signal were too strong to be useable for further material model calibration. Hence, the new high-speed tensile test device (HTTD) is featuring the following three significant functions by design.

- Start-up length to provide a needed force-free travel to accelerate the tensile test machine up to desired speed
- Self-locking wedges to ensure coupling between wedge (specimen) and counter-wedge (machine)
- Local force gauge to measure forces transferred through specimen

The explosion view of HTTD is illustrated in Fig. 2, with a detail of the coupling mechanism between specimen and tensile test machine through self-locking wedges.

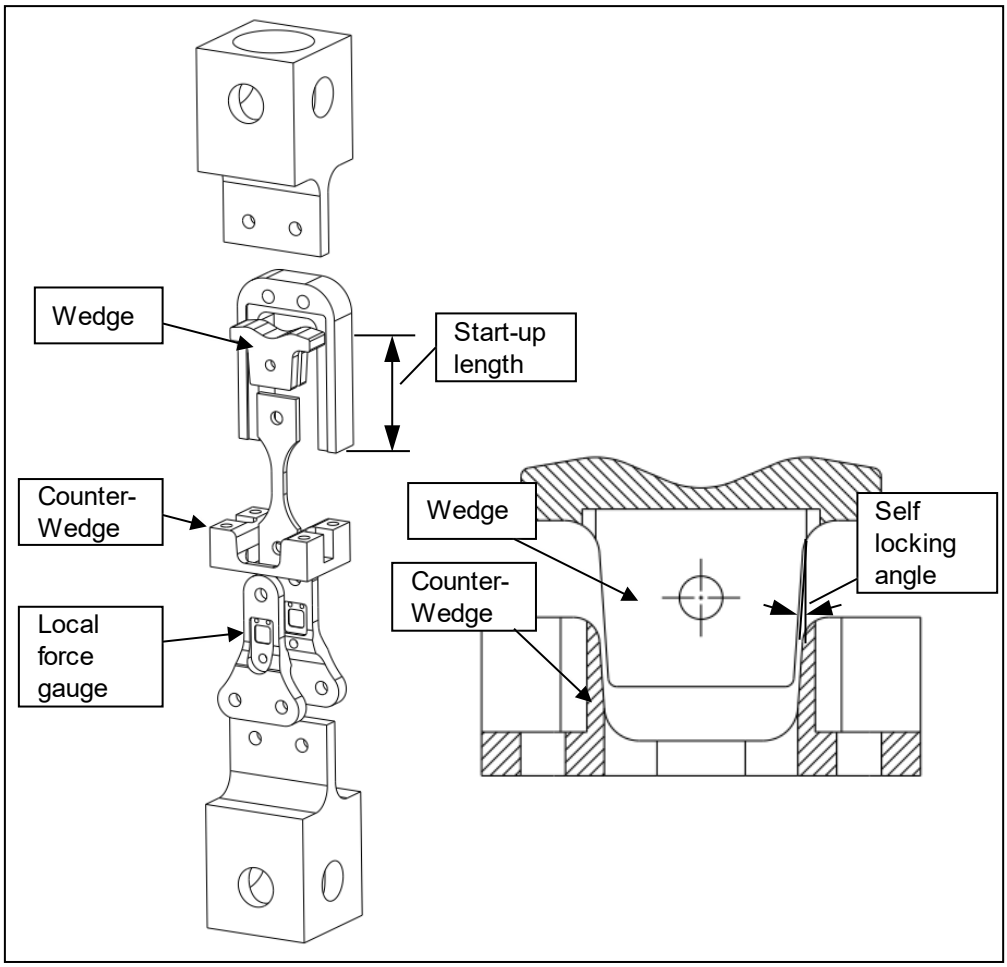

Fig. 2: Explosion view of high-speed tensile test device (HTTD) with a detailed view of self-locking wedge and counter-wedge as coupling mechanism between specimen and tensile test machine.

The following sub-chapter is dedicated to the three significant functional design aspects of the HTTD and will show exemplary results to validate its effects of the above-mentioned design features.

3.1 Significant functional designs of the high-speed tensile test device

To elongate the specimen with a constant velocity, a start-up length needs to be provided, to allow for force-free travel to accelerate the tensile testing machine. It is known from internal investigations, that strain rates of up to $\dot{\varepsilon} = 320\, s^{-1}$ occur during pyrotechnical employments in relevant plastic components. Hence, a tensile test machine speed of $6.4\ \mathrm{m/s}$ is needed, which is derived by the special tensile testing specimen, featuring a clamping length of $20\ \mathrm{mm}$. Thus, a test series is performed to determine the needed travel of the tensile test machine, to accelerate up to $8.0\ \mathrm{m/s}$, giving $40\ \mathrm{mm}$ as a result, where a safety margin is accounted for the moving end.

As the tensile test machine accelerates to the desired velocity, a coupling mechanism needs to ensure load transfer on the specimen. Here, a self-locking wedge is used to couple a wedge to its counter-wedge, where the specimen is mounted. Fig. 3 illustrates for a desired testing velocity of $4.5\ \mathrm{m/s}$, the velocities of tensile test machine (counter-wedge) and of specimen (wedge). It shows the nearly instantaneous load and speed transferal on the specimen.

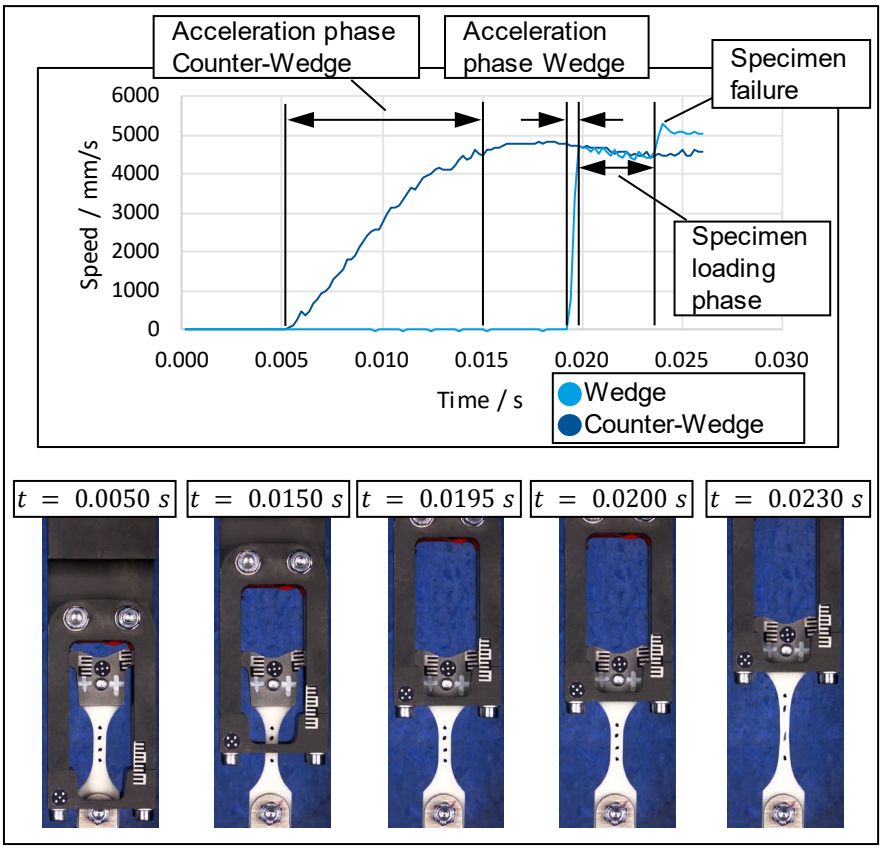

Fig. 3: Acceleration phase of tensile test machine (Counter-Wedge) and acceleration phase of specimen (Wedge) due to self-locking coupling mechanism at desired testing velocity of $4.5\ m/s$.

For determination of forces passing through the specimen, a local force gauge is designed using two strain gauges arranged as *Wheatstone* bridge. One of the two strain gauges is pictured in Fig. 4. Prior to testing, a static calibration test series is performed, correlating the change of voltage of the strain gauge to change in force. Thus, the actual stain within the part is not of interest. Here, two major advantages come into play. First, the force passing through the part is measured very locally, hence the eigenfrequency of the local part is higher compared to the complete test setup. This can be pictured as the complete test setup is to be considered as a serial arrangement of springs. Especially heavy parts, e.g. mounting parts to tensile test machine, decrease the eigenfrequency of the complete test setup. As the force measured locally does not need to travel through the complete test setup, it is not subjected to the oscillations induced by eigenmodes of the test setup. Second, strain gauges show a sampling rate up to $200\ \mathrm{kHz}$, which can resolve very high oscillations. The load cell shipped with the tensile testing machine resolves at $50\ \mathrm{kHz}$. The comparison of the two force signals of strain gauge and tensile testing machine are illustrated in Fig. 4, giving a clear subjective view on the reduction of oscillations due to the local force gauge. It is to be mentioned, that the most ideal, hence showing least oscillations, force signal will be produced, if the force gauge is directly implemented on the tensile specimen. However, as tensile testing is a destructive test technique, this procedure is not feasible.

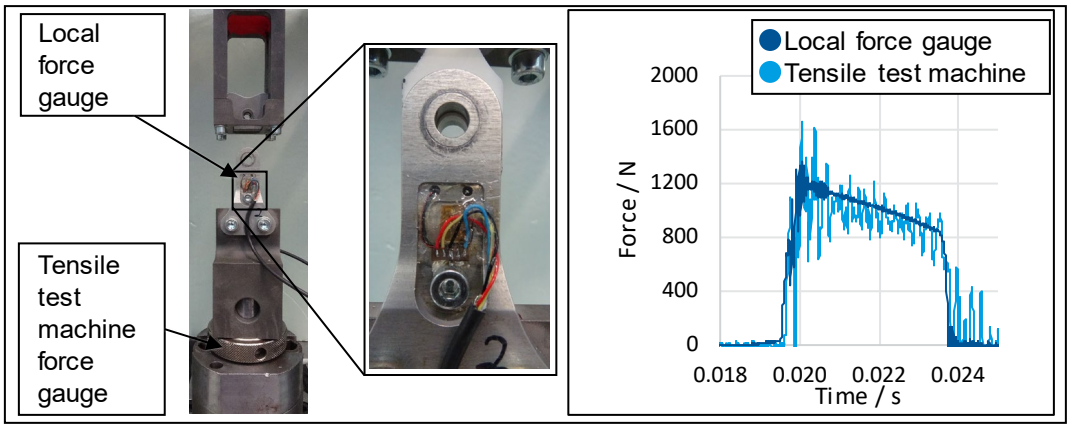

Fig. 4: Local force gauge realized by strain gauges to reduce oscillations in force signal compared to standard force gauge of tensile testing machine.

3.2 Experimental results of high-speed tensile testing device for different loading velocities

The material model calibration process expects a set of three test series on which the material model is calibrated. The three test series differ in loading velocity and are listed in Table 1.

Naming convention	**Loading velocity /** $\mathrm{mm/s}$	**Strain rate acc. to test specimen /** $\mathrm{s^{-1}}$
Quasi-Static (QS)	0.5	0.025
Medium-Speed (MS)	1’100	55
High-Speed (HS)	6’400	320

Table 1: Overview of test conditions for material model calibration process.

The tensile specimens are produces using an inhouse injection molding machine equipped with a mold for the specimen. This gives flexibility for later investigations to determine material scatter due to variance in production parameter as well as scatter from material batch-to-batch.

From all three test series force-displacement characteristics are collected as well as information about the strain field. The strain field as well as displacement information are collected from digital image correlation technique. To apply a simple and fast procedure for information extraction of the strain field, the specimen is marked with contrast areas to derive local strain A_5, global strain A_{15} and lateral strain A_{lat}. The subscript identifies the initial distance of contrast areas as shown in Fig. 5. The extracted relative displacement over time is computed into engineering strain using Eq. 7 , where ε_{eng} gives the engineering strain, Δl the change in length and l_0 the initial length.

$$\varepsilon_{eng} = \frac{\Delta l}{l_0} \qquad \text{Eq. 7}$$

The illustrated test result shows the localization of strains, as the A_5 strain shows a non-linear and stronger increase compared to the A_{15} strain, which shows a linear increase resulting from constant velocity of tensile testing machine.

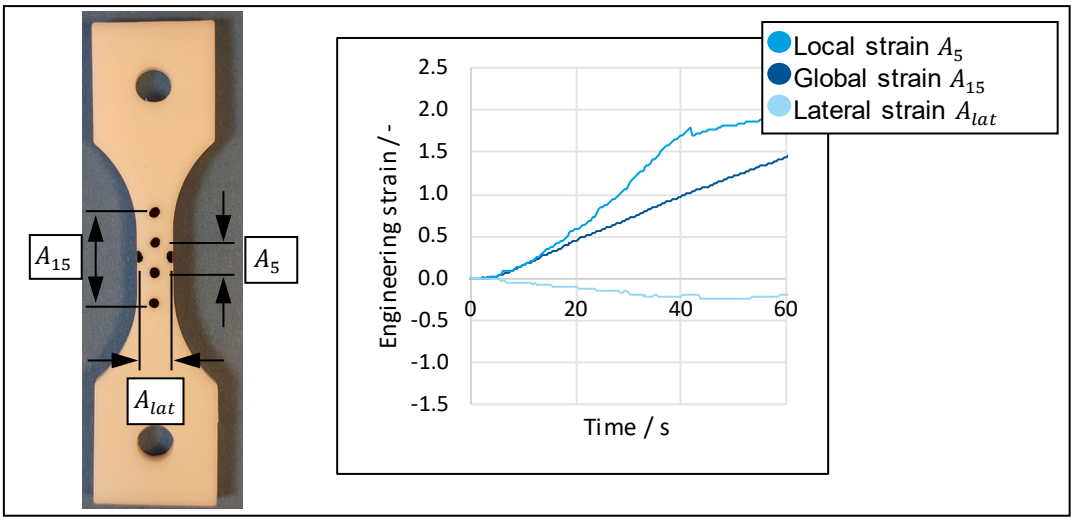

Fig. 5: Markers on tensile specimen for tracing of different strain values A_5, A_{15}, A_{lat}.

3.2.1 Quasi-static tensile test results

According to Table 1, the specimen is loaded with a velocity of $0.5\ \mathrm{mm/s}$, where the functional design features of HTTD are not significant, as the test is considered as quasi-static. The resulting force-displacement curves are listed in Fig. 6, showing successful results as well as an outlier. The outlier showed several material voids on the failure surface, where due to notch effects early failure was induced.

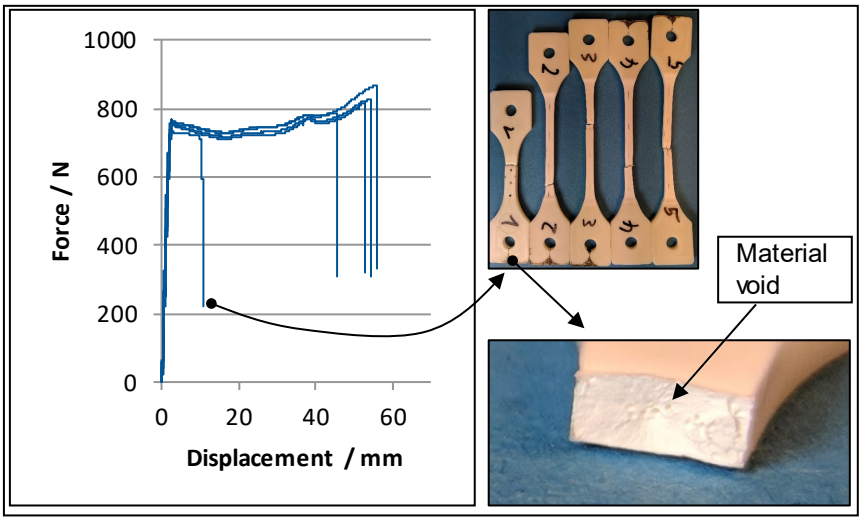

Fig. 6 Force-displacement curves of quasi-static tests showing an outlier due to voids found on the failure area.

3.2.2 Medium- and High-Speed tensile test results

According to Table 1, the specimen where loaded with medium-speed velocity of $1'100\ \mathrm{mm/s}$ and high-speed velocity of $6'400\ \mathrm{mm/s}$. The force signals are listed in Fig. 7 and show both a higher force level compared to Quasi-static testing velocity. This is resulting from strain rate dependent material behavior enforcing material hardening with increasing strain rates. The relative maximum force level increases by $\approx 29\%$ for MS and by $\approx 41\%$ for HS compared to QS.

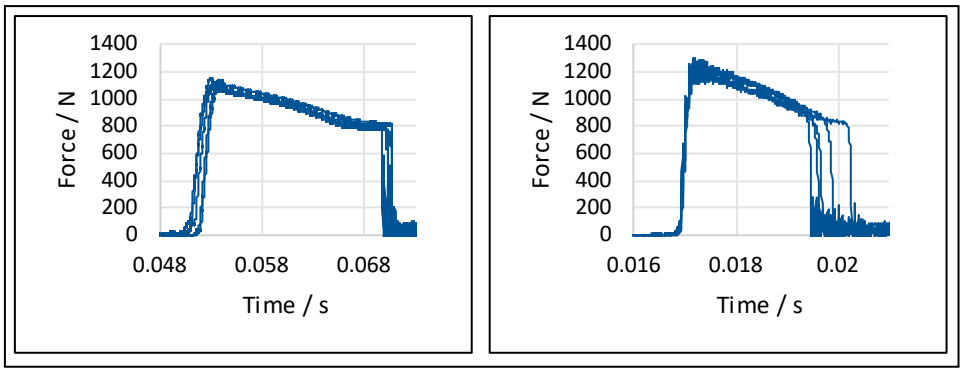

Fig. 7: Force-time curves of tensile tests at medium-speed (left) and high-speed (right). Both datasets are unfiltered data, showing very low oscillations, especially for high-speed results.

3.2.3 Overview of calibration data gathered from QS, MS and HS test velocities

As for all test series force-displacement and strain-displacement characteristics will be used for later material model calibration process. The collected results from testing are illustrated in Fig. 8.

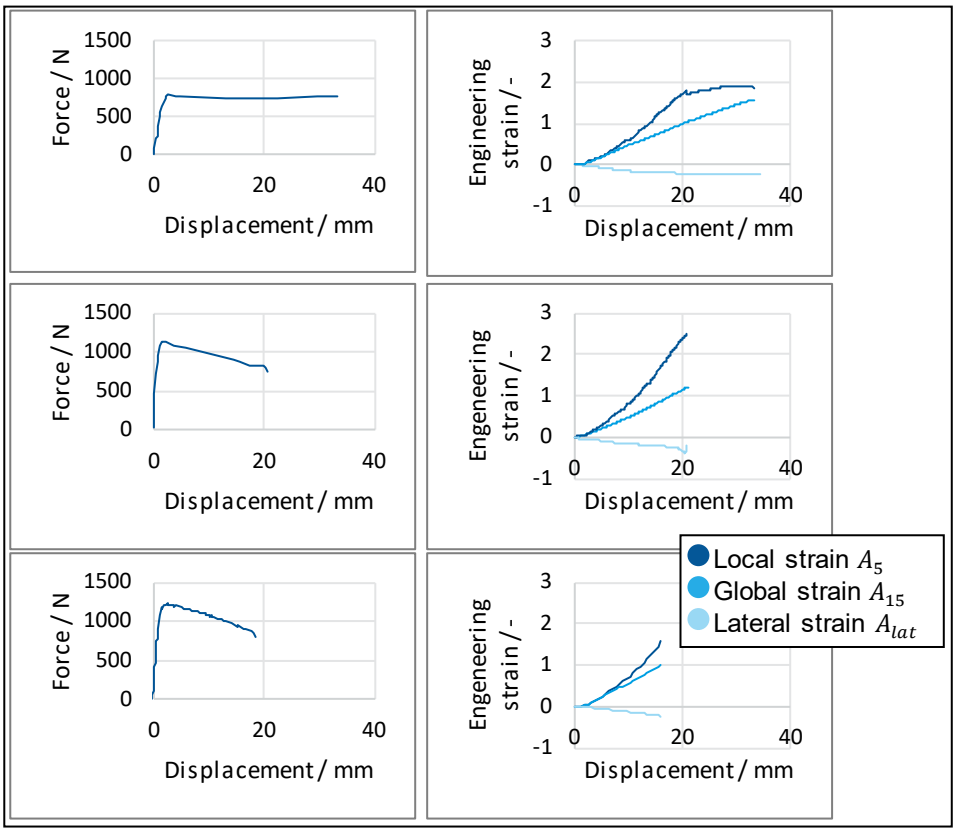

Fig. 8: Overview of calibration data gathered from QS (top), MS (middle) and HS (bottom) test velocities containing force-displacement and strain-displacement characteristics.

Comparing the datasets of force-displacement characteristics, not only the strain rate hardening effect with increasing testing velocity is visible, also the increasing brittleness. Brittleness is described by the decreasing failure displacement as testing velocity is increased. Also noteworthy, the linear characteristic of A_{15} strain for all datasets and non-linear characteristic for A_5 strain. Only for A_5 of QS, the strain showing a saturation after a displacement of $\approx 20\,\mathrm{mm}$. This results from the very large

deformation before failure along with the issue, that contrast areas for A_5 are no longer symmetric with respect to the necking area of the specimen. This is resulting from hardening effect for larger strains at low strain rates. The initially centered area is stretched and hardens. As a certain strain level is reached, other areas with less strain hardening will take up more deformation before failure level is reached. This phenomenon is illustrated in Fig. 9 by the pictured distances l_1, l_2 and l_3.

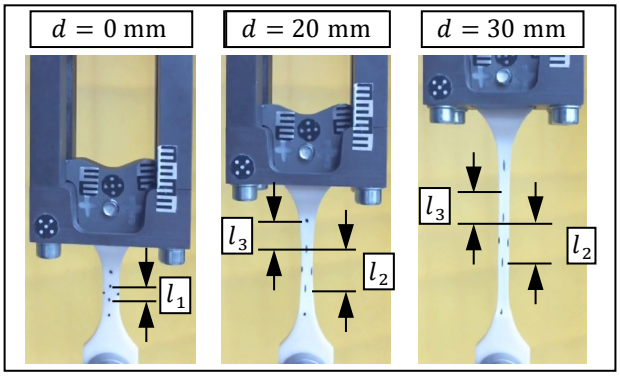

Fig. 9: Allocation of deformation capability of specimen for QS test velocity at high deformation levels. l_2 is not significantly increased for total displacements from $20\,mm$ to $30\,mm$, instead l_3 increases deformation.

Here, l_1 shows the initial length of the strain gauge for A_5. l_2 denotes the length of A_5 at a displacement level of 20 mm, l_3 gives an unspecific length of upper A_5 contrast area to upper contrast area of A_{15} at 20 mm of displacement. As l_2 and l_3 are kept constant in both representations of displacement 20 mm and 30 mm, it can be observed, that l_2 is no longer increased, where deformation is picked up by l_3. Hence, the local strain level is not further increased but the deformation level can still be raised, which is quantified in Fig. 8 for QS test velocity in strain-displacement characteristic.

4 Material model calibration by using test results from high-speed tensile testing device

The experimental results from Chapter 3.2.3 are used to feed the reverse engineering process from Chapter 0 to calibrate the material model. The two-stage process calibrates the quasi-static parameter, such that the area between test- and simulation data curve is minimized. This is performed parallelly with force-displacement and strain-displacement data. Here, a stress-strain response is found, which is basically scaled due to increasing strain rates, whose parameter are found in the second stage of the material calibration process. This is done for force-displacement data and strain-displacement data as multi objective optimization task for medium- and high-speed in parallel. The resulting force-displacement and strain-displacement data in comparison of test- and simulation data is shown in Fig. 10.

The force-displacement characteristic in dependency on the testing velocity is well matching, although there is some potential improvement visible. Especially for medium-speed at low displacements, the simulation force-displacement curve does not meet the strong apex of the test data. Also, for high-speed, the simulation force-displacement curve for displacements between 10 mm and 20 mm is slightly underestimating the test data.

Regarding the strain-displacement data, at quasi-static test velocity, the simulation data misses the full non-linear characteristic of A_5 but follows the s-shaped-slope in general. Same counts for high-speed A_5 strain, where simulation is overestimating the test data. However, as general conclusion, the simulation data does fit satisfyingly good to the test data and shows promising results for force-displacement as well as strain-displacement data.

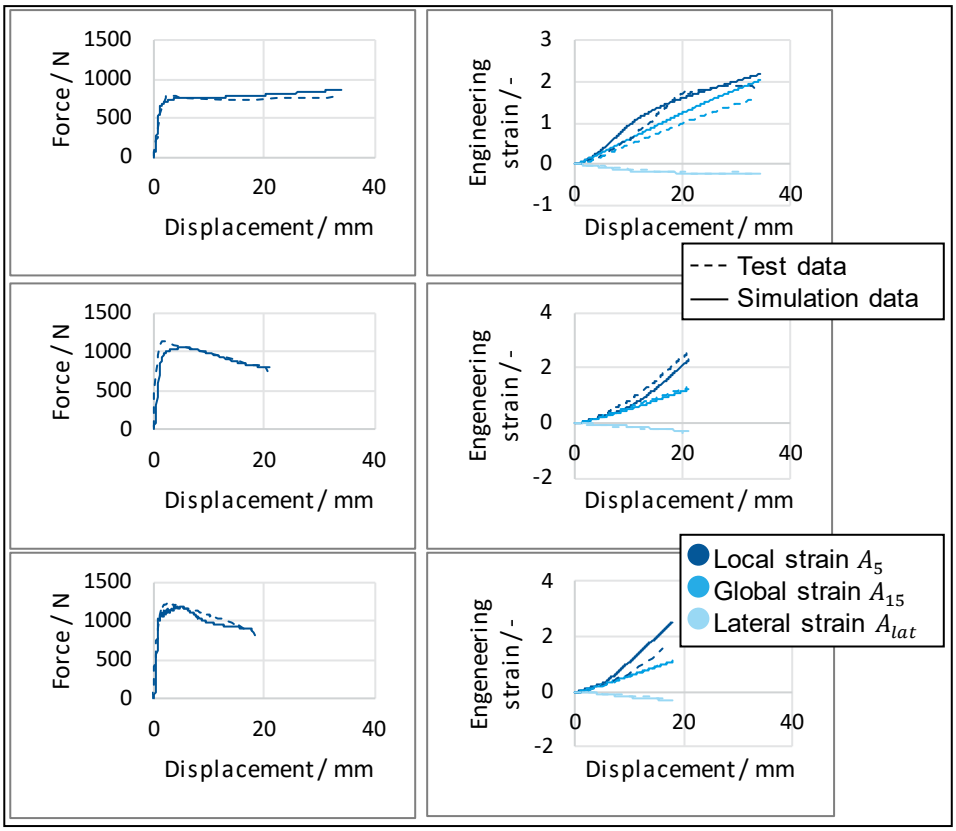

Fig. 10: Comparison of test data (dashed line) versus simulation results (solid line) for quasi-static (top), medium-speed (middle) and high-speed (bottom) test velocities.

The stress-strain response with strain rate dependency is shown in Fig. 11. Here, the quasi-static stress-strain response determines the shape of stress-strain relationship. This shape is basically scaled to match to two higher strain rates.

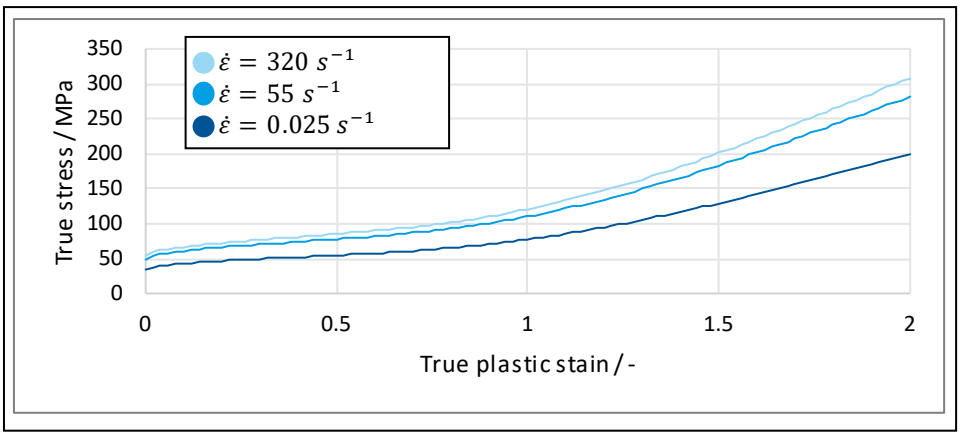

Fig. 11: True stress-strain response determined by material model calibration process considering strain rate dependency.

5 Summary

The current and future trends in automotive industry demand among others the need for a comprehensive simulation material database for thermoplastic materials. This is derived from increased demand for comfort and safety requirements, cost reductions, lightweight design and a faster time-to-market. The here presented two-stage reverse engineering process for automatized material model calibration was developed in earlier works and got improved on several aspects to be able to use accurate test results generated by the newly developed high-speed tensile test device. This is designed to generate test results for strain rates up to $\dot{\varepsilon} = 320\, s^{-1}$, where a self-locking wedge-to-wedge coupling mechanism enables a constant loading velocity of the specimen during stretching. This is realized by a start-up length for acceleration travel of the tensile testing machine. Final significant design aspect of the high-speed tensile test device is the local force gauge, which minimizes oscillations in the force signal especially for high testing velocities. The local force gauge is realized by two strain gauges, which are arranged as *Wheatstone* bridge and which change of voltage is correlated to the change in force passing through the gauge.
The two-stage reverse engineering process is fitting analytical approaches for quasi-static and dynamic stress-strain responses to the test results measured with the high-speed tensile test device. The quasi-static stress-strain response is fitted in the first stage, where in the second stage, the strain rate dependent stress-strain response is fitted along with an analytic approach for modelling of visco-elasticity and strain rate dependent damage. The unknown variables of the analytic approach are determined by a minimization problem, fitting force-displacement and strainfield characteristics from testing to simulation results.
As the reverse-engineering approach is fully automatized, it can be input with test data and after the two-stage iterative process is finished, a calibrated material model will be available.
The presented results, on the one hand from the high-speed tensile test device and on the other hand from the reverse engineering process are very promising and will be very valuable for further enhancing simulation quality and predictability for the design of thermoplastic components in dynamic load cases.

6 Reference

[1] Du Bois, P. et al.: “Implementation of a VE-VP material law for the simulation of energy absorbing thermoplastic components”, 11th European LS-Dyna Conference, Salzburg, 2017

[2] Schilling, S. et al.: "Automatized procedure for characterization and validation of the material behavior of a non-reinforced thermoplastic polymer under dynamic loading", NAFEMS World Conference, Stockholm, 2017

[3] Schilling, S. et al.: "Contribution to an automatized calibration of an analytical visco-elastic and visco-plastic material model of thermoplastic components for simulation of dynamic load cases", Fraunhofer EMI and IWM crashMAT Conference, Freiburg i.Br., 2018